processes

MDPI

Article

Dimer Fatty Acid-Based Polyamide/Organoclays: Structural, Thermal Properties, and Statistical Analysis of Factors Affecting Polymer Chain Intercalation in Bentonite Layers

Afonso D. Macheca [1,2], Diocrecio N. Microsse [2], Theophile M. Mujuri [2], Robert Kimutai Tewo [3], António Benjamim Mapossa [4,5,*] and Shepherd M. Tichapondwa [4]

1 Centre of Studies in Oil and Gas Engineering and Technology, Bairro Luís Cabral (Faculty of Engineering), Eduardo Mondlane University, Av. de Moçambique, Km 1.5, Maputo P.O. Box 257, Mozambique; afomacheca@gmail.com
2 Faculty of Engineering, Eduardo Mondlane University, Av. de Moçambique, Km 1.5, Bairro Luís Cabral, Maputo P.O. Box 257, Mozambique; diocreciomicrosse@gmail.com (D.N.M.); mushitheophile2@gmail.com (T.M.M.)
3 Department of Chemical Engineering, Dedan Kimathi University of Technology, Kiganjo/Mathari, B5, Dedan Kimathi, Nyeri Private Bag 10143, Kenya; kimutaitewo@gmail.com
4 Department of Chemical Engineering, University of Pretoria, Pretoria 0002, South Africa; shepherd.tichapondwa@up.ac.za
5 Department of Chemical and Petroleum Engineering, University of Calgary, 2500 University Drive NW, Calgary, AB T2N 1N4, Canada
* Correspondence: mapossabenjox@gmail.com

Abstract

This work investigates the potential industrial applications of two sodium bentonite samples (white and yellow), obtained from raw Ca-rich bentonite from Maputo Province in Southern Mozambique. Bentonite bio-organoclays were successfully developed from two Mozambican montmorillonite clays through the intercalation of protonated dimer fatty acid-based polyamide chains using a solution casting method. X-ray diffraction (XRD) analysis confirmed polymer intercalation, with the basal spacing (d_{001}) increasing from approximately 1.5 nm to 1.7 nm as the polymer concentration varied between 2.5 and 7.5 wt.%. However, the extent of intercalation was limited at this stage, suggesting that polymer concentration alone had a minimal effect, likely due to the formation of agglomerates. In a subsequent optimization phase, the influence of temperature (30–90 °C), stirring speed (1000–2000 rpm), and contact time (30–90 min) was evaluated while maintaining a constant polymer concentration. These parameters significantly enhanced intercalation, achieving d001 values up to 4 nm. Statistical Design of Experiments and Response Surface Methodology revealed that temperature and stirring speed exerted a stronger influence on d001 expansion than contact time. Optimal intercalation occurred at 90 °C, 1500 rpm, and 60 min. The predictive models demonstrated high accuracy, with R^2 values of 0.9861 for white bentonite (WB) and 0.9823 for yellow bentonite (YB). From statistical modeling, several key observations emerged. Higher stirring speeds promoted intercalation by enhancing mass transfer and dispersion; increased agitation disrupted stagnant layers surrounding the clay particles, facilitating deeper penetration of the polymer chains into the interlayer galleries and preventing particle settling. Furthermore, the ANOVA results showed that all individual and interaction effects of the factors investigated had a significant influence on the d_{001} spacing for both WB and YB clays. Each factor exhibited a positive effect on the degree of intercalation.

Keywords: bentonite; organoclays; surfactants; biopolymer; polyamide

Academic Editor: Anna Wołowicz

Received: 27 May 2025
Revised: 29 June 2025
Accepted: 3 July 2025
Published: 7 July 2025

Citation: Macheca, A.D.; Microsse, D.N.; Mujuri, T.M.; Tewo, R.K.; Mapossa, A.B.; Tichapondwa, S.M. Dimer Fatty Acid-Based Polyamide/Organoclays: Structural, Thermal Properties, and Statistical Analysis of Factors Affecting Polymer Chain Intercalation in Bentonite Layers. *Processes* **2025**, *13*, 2168. https://doi.org/10.3390/pr13072168

1. Introduction

Bentonite is a sedimentary rock commonly classified as claystone or mudstone in geological contexts. It forms cohesive, consolidated deposits, making it suitable for extraction through mining and quarrying, much like other rock materials. Essentially, bentonite is a rock rich in clay or primarily composed of clay minerals, with montmorillonite as its principal component [1–4]. In industrial practice, the terms 'bentonite' and 'montmorillonite' are often used interchangeably. The choice of terminology typically depends on whether the emphasis is on its mineralogical composition or its geological origin and physical properties.

Belonging to the smectite group of minerals, bentonite is among the most widely utilized industrial clays globally, with diverse applications across numerous industries. Its unique physicochemical properties, including high cation exchange capacity, fine particle size, notable swelling behavior, plasticity, rheological characteristics, adsorption capacity, lubrication, and bonding strength, make it an indispensable material in sectors such as petroleum drilling, cement manufacturing, environmental remediation, civil engineering, bleaching earth, foundries, cosmetics, pharmaceuticals, agriculture, coatings, and paper production [1–11].

Formed primarily through altering volcanic ash and tuff, bentonite is generally classified based on its dominant interlayer cations as sodium and calcium-bentonite. Sodium bentonite (Na-bentonite), typically of marine origin, exhibits superior swelling capabilities, whereas calcium bentonite (Ca-bentonite), more common in freshwater environments, is often non-swelling [12–14]. Despite its versatility, natural bentonite has inherent limitations for specific applications where surface functionality and interlayer compatibility with organic molecules are crucial.

Chemical modifications, particularly the development of organoclays, have been extensively studied as a means of addressing the above inherent limitations of natural clays, such as their hydrophilicity and limited compatibility with organic matrices. Organoclays are a class of modified clays in which the naturally occurring inorganic exchangeable cations, typically Na^+ or Ca^{2+}, within the interlayer spaces of smectite-type clays such as montmorillonite are replaced with organic cations, typically long-chain alkylammonium ions derived from quaternary ammonium salts. This ion-exchange reaction not only renders the clay surface more organophilic (hydrophobic), facilitating its dispersion in nonpolar media, but also expands the interlayer spacing (basal spacing or d-spacing), allowing the intercalation of larger organic molecules [15–17].

This tailored modification significantly enhances the compatibility of the clay with a variety of organic systems and broadens its application potential. Organoclays are now widely used in water treatment (for adsorbing hydrophobic contaminants), polymer nanocomposites (as nanofillers improving mechanical and barrier properties), paints and coatings (as rheological modifiers), adhesives (for thermal and mechanical reinforcement), and oil drilling fluids (for controlling rheology and improving thermal stability) [18–22].

Extensive research has focused on the synthesis and utilization of organoclays, particularly those modified with long-chain quaternary ammonium salts, cationic surfactants of the type $[(CH_3)_3NR]^+$ or $[(CH_3)_2NR]^+$, where R denotes alkyl or hydroxyl chains [18,23–40]. However, concerns regarding their environmental persistence and potential health hazards, such as dermal irritation, have prompted the search for more sustainable alternatives.

Instead of relying on traditional cationic surfactants, the research team has explored a surfactant-free organo-modification approach using biodegradable polymers derived from plant oils, such as soybean oil. This method involves solution intercalation, which operates on the principle of ion exchange by substituting inorganic ions with organic ones. The

focus has been on bio-based polyamides bearing terminal amine groups, with dimer fatty acid-based polyamides serving as a key example.

The surfactant-free organo-modification method, previously detailed in our earlier studies [41–43], involves the use of dimer fatty acid-based polyamides, which are bio-based polymers of low molecular weight that are soluble in various organic solvents. These polyamides possess amine end groups that become protonated in appropriate carboxylic acids, enabling the direct intercalation of polymer chains into clay layers via the solution casting method. This suggests that organo-clays can be prepared without the need for conventional surfactant-based organo-modification.

Structurally, dimer fatty acid-based polyamides are composed of over 99% triglycerides. These amorphous co-polyamides are synthesized by dimerizing unsaturated vegetable fatty acids. The resulting dimer acids are then reacted with other diacids and selected aliphatic diamines through polycondensation to produce the target polyamides [41]. Further details on the intercalation technique and polymer-based organoclays synthesis are provided in the Materials and Methods section.

Building upon previous research conducted by our group on polymer-clay nanocomposites [41–43], which focused on elucidating intercalation mechanisms within polymer matrices, this study optimizes the organo-modification process. Using Statistical Design Modeling and Response Surface Methodology (RSM), key parameters affecting polymer intercalation into bentonite, namely temperature, polymer content, contact time, and stirring speed, were investigated. Due to their accessibility and relevance, two bentonite samples from Mozambique were selected.

The research seeks to validate a novel, sustainable organo-modification technique and demonstrate its potential for producing high-performance, biodegradable organoclays. The outcome will offer a viable, eco-friendly alternative to conventional surfactant-based materials, supporting current environmental imperatives while expanding the technological options available in sectors dependent on organoclay functionalities.

2. Materials and Methods

2.1. Materials

Two sodium bentonite samples (white and yellow), obtained from raw Ca-rich bentonite collected in the Boane region of Maputo Province, Southern Mozambique, were pre-activated with Na_2CO_3 in our laboratory. Their chemical compositions are presented in Table 1 [44]. The deposit is located approximately 40 km southwest of Maputo City, on the slopes of Montes dos Pequenos Libombos and about 9 km from the Boane district headquarters. It is accessible via the Maputo–Namaacha and Maputo–Ressano Garcia roads, as well as by smaller trails. The raw bentonite is extracted through open-pit mining over an area of around 40,000 m^2, specifically in the "Depósito Cooperativa 1" and "Depósito Cooperativa 2" [34]. The purification and Na_2CO_3 activation procedures followed the methodology described in our earlier work [44]. The white and yellow bentonite clay samples were labelled WB and YB, respectively. Acetic acid (glacial, 100% purity; CAS No. 64-19-7) and sodium carbonate (CAS No. 497-19-8) were procured from Merck Chemicals (Pty), located in Germiston, Gauteng Province, South Africa, and supplied by Tecnotraguas-Mozambique. Both reagents were used as received. The amorphous co-polyamide (dimer fatty acid polyamide), Euremelt 2140 (E2140), was supplied by Huntsman Advanced Materials (Deutschland) GmbH & Co. KG, Trottäcker, Bad Säckingen, Germany.

Table 1. Chemical composition of white and yellowish bentonite clays.

Sample	Composition (wt.%)									
	SiO_2	Al_2O_3	Fe_2O_3	CaO	K_2O	Na_2O	MgO	MnO	TiO_2	P_2O_5
WB	79.6	13.4	2.52	0.49	0.21	0.64	2.97	0.01	0.17	0.01
YB	68.7	9.74	2.32	0.35	0.24	0.76	2.05	0.01	0.12	0.01

2.2. Preparation of Organoclays

The preparation of organoclays was done in two main stages, based on an adaptation of the method proposed by Macheca et al. [41] and Macheca et al. [42]. In the first stage, three samples of each clay type, white and yellow, were prepared with polyamide at concentrations of 2.5, 5.0, and 7.5 wt.%. Key process parameters, including temperature (30 °C), contact time (30 min), and stirring speed (1000 rpm), were kept constant in all the experiments carried out.

The preparation procedure involved dissolving a measured amount of polyamide in acetic acid to create a 10 wt.% polyamide solution. Separately, a 500 mL stainless steel container was mixed using a shear mixer at room temperature for 5 min. The 10 wt.% dropwise additions of polyamide solution were made to the mixture. Once the addition was complete, mixing continued for an additional 25 min. Next, distilled water was added during stirring to help loosen the clay structure. This was followed by a seven-day washing process to remove excess acetic acid, during which the water was replaced daily. The organo-modified clays were then separated by decantation and dried for 48 h at 60 °C in an oven. The resulting polymer-modified clays were labeled according to their composition: WBxPA for white bentonite and YBxPA for yellow bentonite, where "x" indicates the polymer concentration (2.5, 5.0, or 7.5 wt.%) and "PA" denotes polyamide. For example, WB2.5PA refers to white bentonite modified with 2.5 wt.% polyamide. Neat polyamide polymer was also subjected to the same procedure to prepare the sample used for property comparisons, specifically for XRD and TGA analysis.

The second stage focused on optimizing the organo-modification process by enhancing polymer chain intercalation within the bentonite layers. Unlike the first stage, this phase involved varying three key parameters: temperature (30–90 °C), contact time (30–90 min), and stirring speed (1000–2000 rpm), while keeping the polymer concentration constant. The sample from the first stage that exhibited the highest degree of intercalation was measured by the basal spacing (d001) using Bragg's Law. Optimization was performed using the Statistical Design of Experiments (DOE) approach.

2.3. Characterization Methods

Elemental composition of bentonites and structural analysis of composites (polymer-based organoclays), including neat polymer, were performed using a multifunctional equipment X-ray diffraction (XRD)/XRF model PANalytical X'Pert Pro from Malvern Panalytical Company (Malvern, UK) equipped with an X'Celerator detector. Using X'Pert High Score Plus software 5.1, mineralogy was determined by the pattern that best fits the measured diffraction pattern from the ICSD database. Thermogravimetric analysis (TGA) of bentonites and their polymer-modified hybrids, including neat polymer, was done using a model Perkin Elmer 4000 TGA equipment, from PerkinElmer, Inc. (Waltham, MA, USA). The test was conducted in an open 150 µL alumina pan filled with roughly 15 mg of the sample, under an airflow rate of 50 mL/min, at a temperature range of 25 °C to 950 °C, under a heating rate of 10 °C/min. The SEM images were performed at 1 kV resolution, using Zeiss Ultra 55 FESEM Field from Carl Zeiss AG Company (Oberkochen, Germany). The composites were coated with carbon before SEM analysis. The surface area was calculated by the BET method [45]. Particle size results were also obtained from

BET analyses. Except for XRD, all the characterization techniques discussed were applied exclusively to samples prepared during the first stage.

2.4. Statistical Design of Experiments

Full Factorial Design

A 2^k full factorial design was used to investigate the factors and their interactive effects on the extent of polymer chain intercalation into the bentonite galleries, as measured by the basal spacing (d_{001}) [46–48]. Factors such as temperature, polymer content, contact time, and stirring speed were taken as the independent variables (k = 3) and d_{001} as the dependent variable (response). A low level denoted the least number of factors employed, while a high level showed the highest number of factors. The factor levels were recorded as − (low-level) and + (high-level). Each of the three components' center points was coded as "0," as shown in Table 2.

Table 2. Factorial levels using central composite design for d_{001}.

Factors	Symbol	Coded Levels		
	−	**−1**	**0**	**+1**
A: Temperature, °C	X_1	30	60	90
B: Contact time, min	X_2	30	60	90
C: stirring speed, rpm	X_3	1000	1500	2000

Given the current focus on the central point of the factors, a second-order statistical design of experiments is appropriate, and the following equation best represents this model:

$$Y = \beta_0 + \sum_{i=1}^{k} \beta_i X_i \sum_{i=1}^{k} \beta_{ii} X_i^2 + \sum\sum_{i<j} \beta_{ij} X_i X_j + \varepsilon \quad (1)$$

where X_i is the coded factors, ε is the error, β_0 is the offset term, β_i is the linear effect, β_{ii} is the squared effect, β_{ij} is the interaction effect, and Y is the expected response.

The optimal conditions for the organo-modification process were determined using Response Surface Methodology (RSM) with a central composite design (CCD) [44,46–48]. Equation (1) describes the degree of intercalation, representing the actual functional linkage between the polymer chains and the bentonite layers, as a function of the independent variables and their interactions. The central composite design is derived from a 2^k factorial design by adding six axial points, coded as $\pm\,\alpha$, along with nine axial center locations where all factors are set to zero. The value of α is determined via Equation (2):

$$\alpha = \left(2^k\right)^{1/4} \quad (2)$$

where K represents the quantity of components. Considering there are three variables in this investigation, thus α is 1.682.

The lower $-\alpha$ (Z_i,$-\alpha$) and upper $+\alpha$ (Z_i,$+\alpha$) positions, which represent the realistic variable's levels determined by Equations (3) and (4):

$$Z_{i,+\alpha} = Z_{i,0} + \alpha\Delta_i \quad (3)$$

$$Z_{i,-\alpha} = Z_{i,0} - \alpha\Delta_i \quad (4)$$

where Δ_i represents the center, or basic levels, and $Z_{i,0}$ is the factor's variation range, parameters calculated by Equations (5) and (6):

$$Z_{i,\,0} = 1/2(Z_{i,1} + Z_{i,2}) \quad (5)$$

$$\Delta_i = 1/2(Z_{i,1} - Z_{i,2}) \quad (6)$$

where the factors' upper and lower levels are denoted by $Z_{i,1}$ and $Z_{i,2}$.

The central composite design, showing the corresponding combinations of independent variables, is listed in Table 3. Components (Z_1, Z_2, and Z_3) represent the realistic variable values, corresponding to temperature (°C), contact time (min), and stirring speed (rpm), respectively. The connection between the actual values ($Z_{1,j}$) and the coded values ($X_{i,j}$) is expressed by Equation (7):

$$Z_{i,j} = Z_{i,0} + \Delta_i X_{i,j} \quad (7)$$

Table 3. Central composite design matrix for d_{001}.

Run	Z_1	Z_2	Z_3
1	90	90	2000
2	30	90	2000
3	90	30	2000
4	30	30	2000
5	90	90	1000
6	30	90	1000
7	90	30	1000
8	30	30	1000
9	110.46	60	1500
10	9.54	60	1500
11	60	110.46	1500
12	60	9.54	1500
13	60	60	2341
14	60	60	659
15(C)	60	60	1500
16(C)	60	60	1500
17(C)	60	60	1500
18(C)	60	60	1500
19(C)	60	60	1500
20(C)	60	60	1500
21(C)	60	60	1500
22(C)	60	60	1500
23(C)	60	60	1500

(C) = Axial center points.

From Equations (3)–(6), $Z_{i,+\alpha,}$ and $Z_{i,-\alpha}$ levels were calculated, and are summarized in Table 4. Analysis of variance (ANOVA) was used to design and analyze the experimental data using StatSoft Statistica software, version 8.0.360.0 (English), Palo Alto, CA, USA. The interaction of independent factors was studied using RSM. The *p*-value with a 95% confidence level was used to determine whether to accept or reject the model terms. Coefficient R^2 represented the statistical design model's quality of fit.

Table 4. Use of central composite design for the factors coded and actual levels for d_{001}, applying RSM.

Factors	Coded and Real Levels				
	$-\alpha$	−1	0	+1	$+\alpha$
A: Temperature, °C	9.54	30	60	90	110.46
B: Contact time, min	9.54	30	60	90	110.46
C: Stirring speed, rpm	659	1000	1500	2000	2341

3. Results and Discussion

3.1. X-Ray Diffraction (XRD)

The XRD patterns of the neat PA, starting with the white and yellow bentonites (WB and YB), and polymer-based organoclays are shown in Figure 1. As expected, the XRD pattern of neat dimer fatty acid-based polyamides displays a broad amorphous halo [41], and the polymer-modified bentonite hybrids exhibit a characteristic (001) peak, indicating intercalation of polymer chains into the clay layers and structural organization absent in the neat polymer. From the figure, it is clear that clays exhibited d001 reflections corresponding to 1.48 nm for white bentonite and 1.46 nm for yellow bentonite, which is typical of clays containing an exchangeable cation of Na^+ and Ca^{2+} [14]. The presence of Ca^{2+} ions in both bentonites reflects their natural calcium saturation, typical of Boane bentonites [49–51], while the presence of Na^+ results from the modification process with Na_2CO_3 applied to the bentonites. The asymmetric broadening of the d_{001} reflection in the white bentonite suggests reduced crystallinity, limited swelling capacity, and lower hydration power compared to the yellow bentonite [18,52].

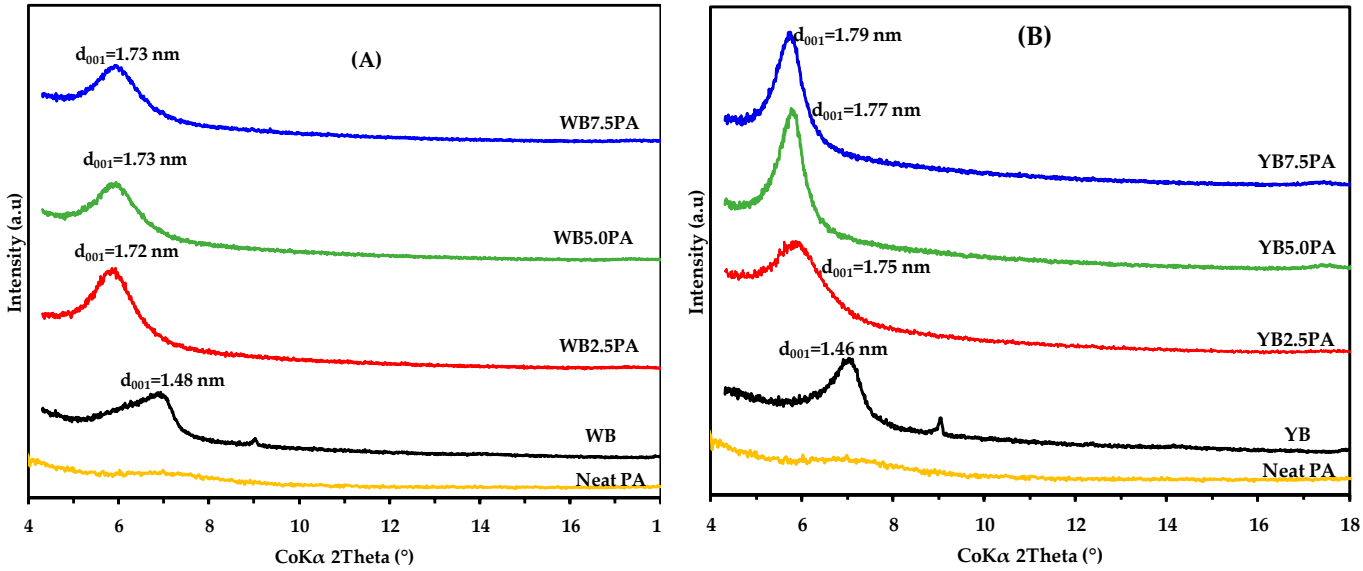

Figure 1. X-ray diffraction spectra of the neat PA, starting white bentonite-WB (**A**), yellow bentonite-YB (**B**) and their polymer modified hybrids corresponding to 2.5 wt.%, 5.0 wt.%, and 7.5 wt.%.

The basal spacing values of the polymer-modified samples increased from 1.48 nm to a maximum of 1.73 nm for white bentonite (Figure 1A) and from 1.46 nm to a maximum of 1.79 nm for yellow bentonite (Figure 1B) as the polymer content was varied from 2.5 wt.% to 7.5 wt.%. This increment behavior suggests that treatment with protonated dimer fatty acid-based polyamide chains affected the clays. From the configuration structure, the d_{001} values of 1.73 nm and 1.77 nm observed for the two organo-modified clay samples (WB and YB) suggest the appearance of two layers of ions in the interlamellar region [32,53], which typically show a basal spacing d_{001} of 1.70 nm.

No significant changes were observed in d_{001} across the three polymer contents (2.5 wt.%, 5.0 wt.%, and 7.5 wt.%) for both WB and YB samples. However, the yellow bentonite sample has a slightly larger d_{001} than that of the white bentonite sample, suggesting that the yellow bentonite gives a better response to polymer modification. The higher cristobalite (SiO_2) content in white bentonite (35.1 wt.%) compared to yellow bentonite (23.3 wt.%) [50,54] may explain the lower response of white bentonite to polymer treatment.

3.2. Thermogravimetric Analysis (TGA)

TGA curves for the neat WB, YB, and their polymer-modified hybrids are shown in Figure 2A,B. Only two major thermal events were observed in the TGA curves of neat polyamide. The first stage of degradation involved major mass loss, commencing at about 350 °C. Above 350 °C, the neat polymer showed a rapid mass loss. The polymer was then completely oxidized to volatile products between 600 and 900 °C. Both neat clays, white bentonite (WB) and yellow bentonite (YB), demonstrated similar thermal behavior across the temperature range, showing four distinct regions of mass loss, characteristic of smectite clays [14]. The first mass loss, between 20 °C and 100 °C, correlates with the free water released from the clay surface. Between 100 °C and approximately 400 °C, the mass loss is ascribed to the interlayer water and organic matter. The subsequent loss between 400 °C and 700 °C is due to the dihydroxylation of aluminosilicates [55]. Finally, mass loss beyond 700 °C results from the decomposition of the clay's crystal lattice, leading to the formation of a new crystalline phase [7,14]. As expected, the polymer-modified hybrids from both clay families exhibited a higher mass loss above 400 °C than their unmodified counterparts. This increased mass loss is due to the decomposition of the polyamide. The breakdown of organic species is typical of organic molecules when they are adsorbed onto the surface of clay layers [56].

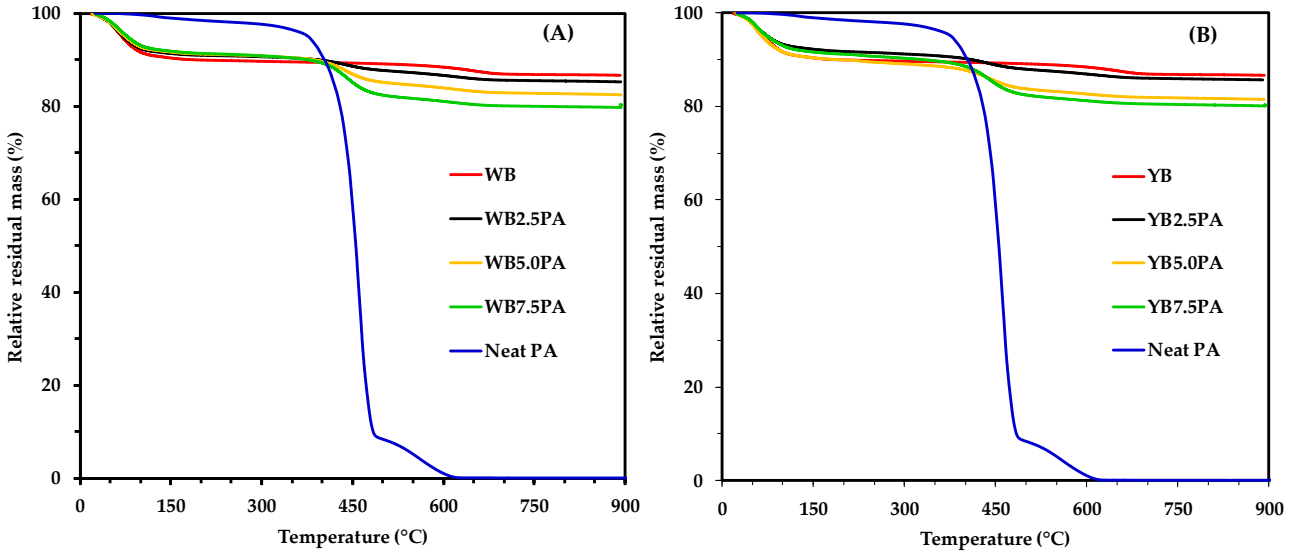

Figure 2. TGA curves of the neat PA, starting white bentonite—WB (**A**), yellow bentonite—YB (**B**) and their polymer modified hybrids corresponding to 2.5 wt.%, 5.0 wt.%, and 7.5 wt.%.

Figure 2 also shows that the organoclay samples were more stable than neat polyamide under thermo-oxidative degradation conditions. The formation of the composite through the mixing of clay and polymer appears to enhance thermal stability. This improvement is likely due to the barrier effect of the clay, which hinders oxygen diffusion into the composite matrix and restricts the release of small molecular fragments produced during thermal decomposition [41]. These findings corroborate the XRD results, which indicated minimal changes in the d-spacing of the polymer-modified clays.

3.3. SEM Micrographs

Figure 3 indicates the SEM images of the neat white bentonite and composites. The starting clay sample shows rounded, nano-sized particles with some pseudo-hexagonal crystalline edges and varying degrees of roughness. Additionally, irregularly shaped aggregates are also visible. The polymer-modified hybrids display similar morphologies to the neat bentonite. However, in the modified samples, the aggregates are larger and more wrinkled. The agglomerate size increases with rising polymer concentration, suggesting poor compatibility between the clay nanoparticles and the polymer matrix. Higher polymer concentrations have a more compact clay surface, reflecting the clay's hydrophobic character. Compared to untreated bentonite, the hydrophobized clay particles exhibit a stronger tendency to cluster, as the polymer chains neutralize the clay's negative charge and reduce electrostatic repulsion between layers [57]. This agglomeration behavior supports the idea that much of the polymer adsorbs onto the clay surface at higher concentrations. This is consistent with the use of acetic acid, which has a dielectric constant that is lower than water [41], allowing protonated amine groups on the polyamide chains to disperse the clay's surface charges in the mixture. The increase in aggregate size in polymer-modified clay samples could also be due to the surface energy incompatibility of uncoated silica nanoparticles and polymer-coated bentonite flakes [34].

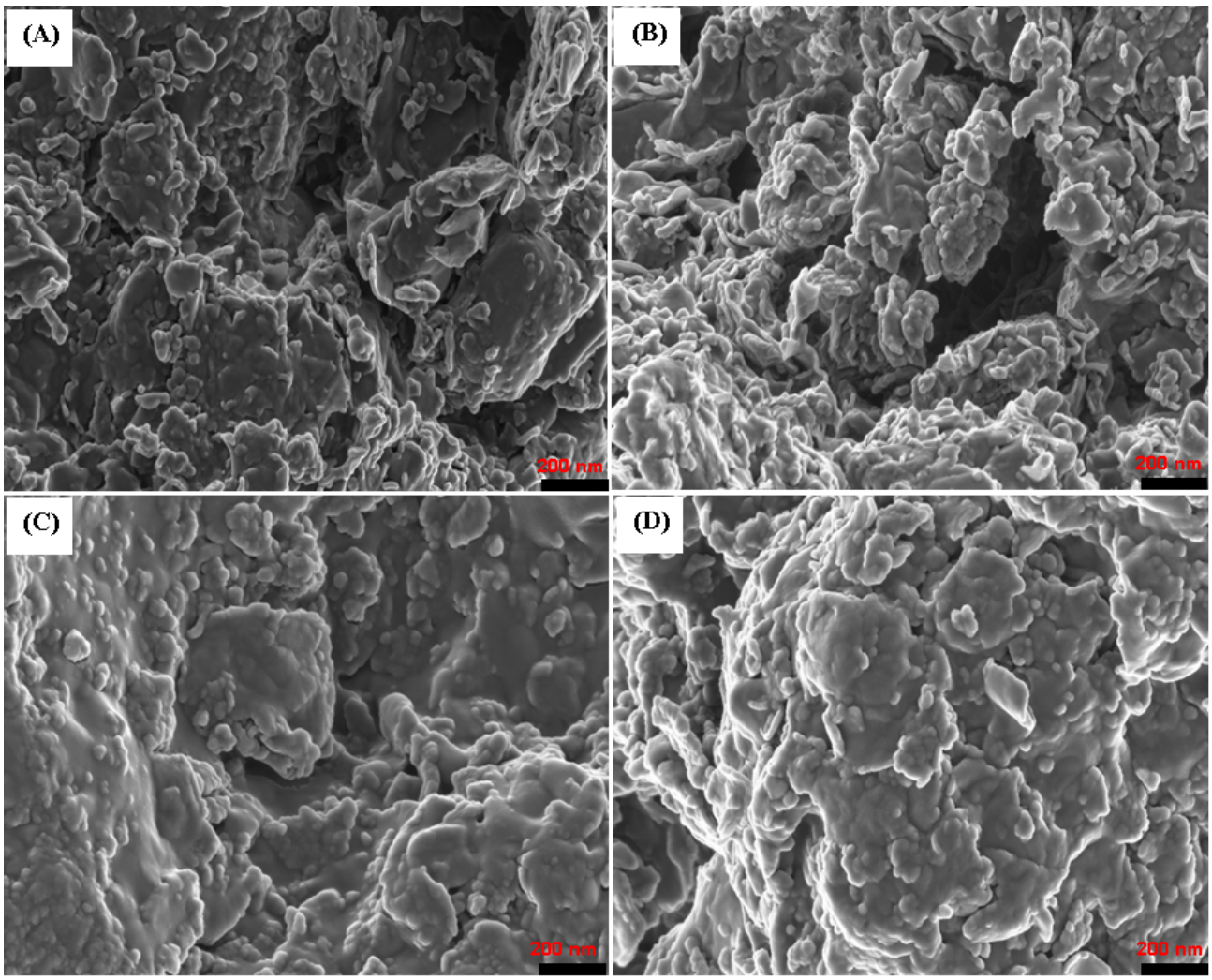

Figure 3. SEM micrographs of the starting and modified bentonite clays. (**A**) Starting with white bentonite, (**B**) WB2.5PA, (**C**) WB5.0PA, and (**D**) WB7.5PA.

Figure 4 shows SEM images of the yellow bentonite and its polymer-modified hybrids at different loadings. The unmodified yellow bentonite has a heterogeneous surface morphology characterized by irregularly shaped, nano-sized particles forming loosely packed aggregates. Similar to the white bentonite, some pseudo-hexagonal edges and flaky structures are observed. Upon polymer modification, the yellow clay exhibits an increase in aggregate size and surface wrinkling, particularly at higher polymer concentrations (5.0 wt.% and 7.5 wt.%). These features indicate increased interparticle interactions and partial exfoliation, consistent with reduced electrostatic repulsion and enhanced hydrophobic interactions induced by the polymer matrix. Despite minor textural differences, the overall morphological behavior of yellow bentonite composites closely resembles that of the white clay hybrids.

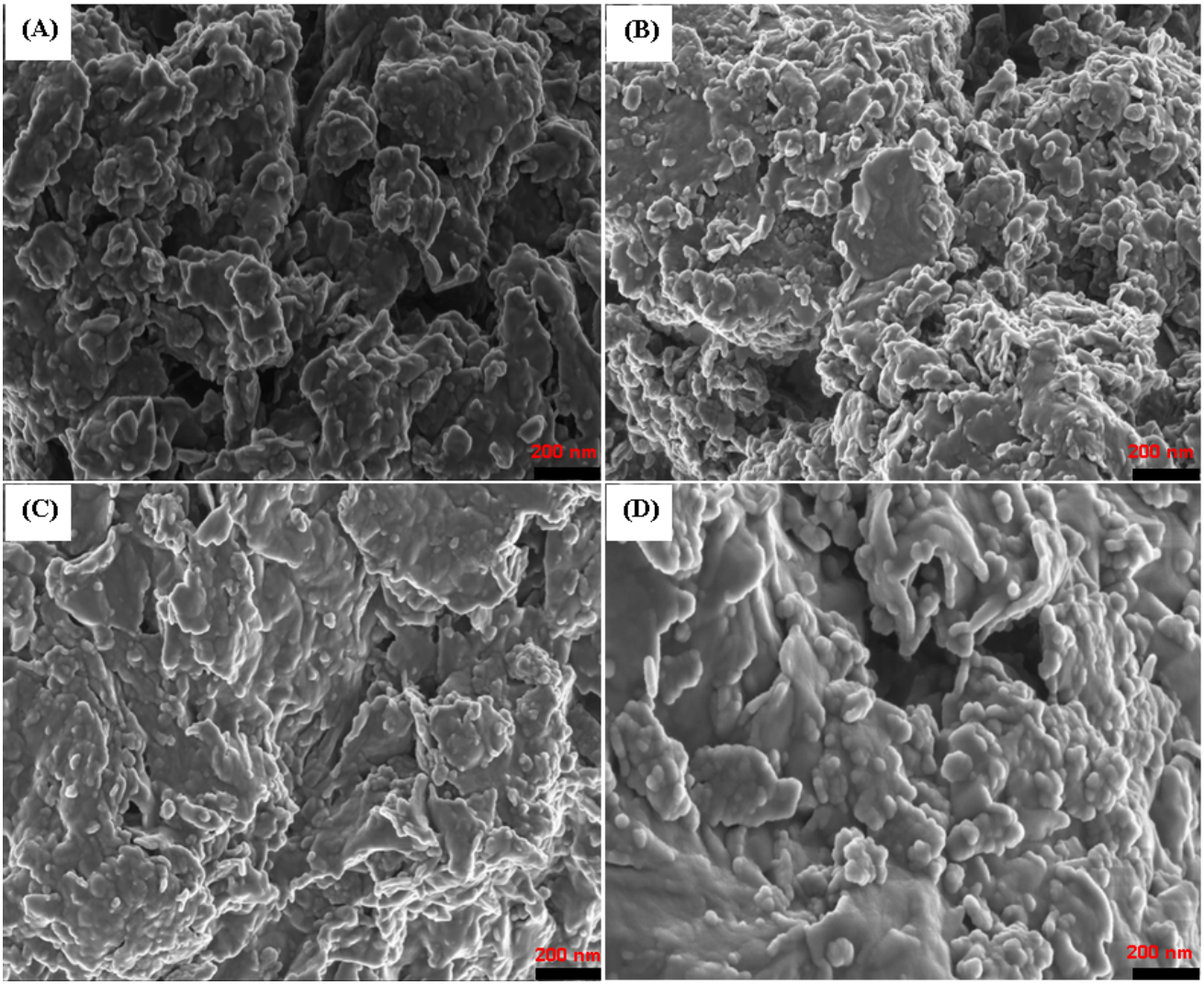

Figure 4. SEM micrographs of the starting and modified bentonite clays. (**A**) Starting yellow bentonite, (**B**) YB2.5PA, (**C**) YB5.0PA, and (**D**) YB7.5PA.

3.4. BET Surface Area, Particle Size and Pore Volume

Table 5 summarizes the BET specific surface area, particle size, and pore volume of both white and yellow bentonite samples. Across all polymer-modified hybrids, a consistent trend was observed relative to the unmodified clays: both BET surface area and pore volume decreased significantly, with the reduction being more pronounced in the yellow bentonite. At a polymer concentration of 7.5 wt.%, the surface area of the yellow

bentonite decreased by nearly 2.5 times, while its pore volume declined by approximately 1.7 times. Despite these reductions, the values remained within the acceptable range for technological applications. This behavior is attributed to the adsorption of polymer chains onto the clay particles, forming a coating layer. As the polymer concentration increased, this layer became more uniform and thicker, likely accounting for the progressive decline in BET surface area and pore volume with higher polymer loadings [38].

Table 5. BET surface area, particle size, and pore volume of the natural and modified bentonite clays.

Clay Type	Surface Area (m^2/g)	Particle Size (nm)	Pore Volume ($cm^3\ g^{-1}$)
WB	43.39	77.06	0.147
WB2.5PA	39.24	109.48	0.129
WB5.0PA	37.12	138.42	0.116
WB7.5PA	31.69	150.49	0.109
YB	46.12	50.02	0.088
YB2.5PA	35.39	128.04	0.068
YB5.0PA	24.91	146.48	0.062
YB7.5PA	18.12	172.10	0.052

Regarding particle size, the organo-modification process affected the white and yellow bentonites. The particle size increased with higher polymer concentrations. For white bentonite, the particle size grew from 77.00 nm to 109.48 nm, 138.42 nm, and 150.49 nm for polymer-modified hybrids with 2.5 wt.%, 5.0 wt.%, and 7.5 wt.% polymer, respectively. A similar pattern of increasing particle size was observed for hybrids derived from yellow bentonite. However, yellow bentonite exhibited a higher affinity for the polymer. At 7.5 wt.% PA, the particle size of yellow bentonite increased nearly threefold compared to the original sample, while the particle size of white bentonite increased by almost twofold. This difference may be due to the higher silica content in white bentonite (79.6%) compared to yellow bentonite (approximately 68.7%). The particle size increase for all polymer-modified hybrids is due to polymer adsorption on the clay surface, leading to aggregation and formation of larger hybrid structures.

3.5. Screening of Factors for d_{001}

Figure 5 illustrates Pareto charts of the standardized effects at the p = 0.05 level of significance for both WB and YB clay families, in which values above 0.05 indicate significant effects. The results show that all independent factor terms, whether linear and quadratic, and their interactions, significantly affect the extent of intercalation in polymer chains, with 95% confidence. The linear terms' significance for the two clay families follows the order: temperature > stirring speed > contact time, while the quadratic terms' significance is in the order: stirring speed > contact time > temperature. The significance of the combined or interaction effects appears in the following order: temperature/stirring speed > temperature/contact time > contact time/stirring speed.

Tables 6 and 7 show the ANOVA results for the interaction influences of the factors on d_{001} for WB and YB, respectively. All factor effects, for both individual and interaction, were found to significantly influence the degree of intercalation in both clay types (WB and YB), as they all exhibited positive signs, consistent with the Pareto charts presented in the previous section.

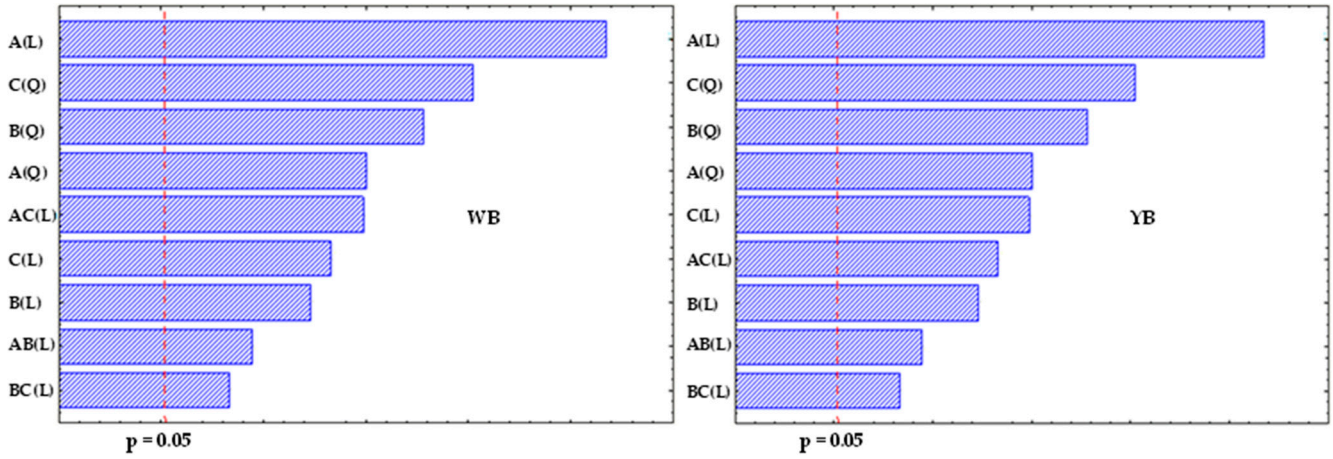

Figure 5. Pareto charts of the standardized effect of the degree of polymer chain intercalation of WB and YB.

Table 6. ANOVA results for d_{001} of WB.

Term	DF	SS	MS	F	*p*-Value
X_1	1	4.7295	4.7295	47,294.67	0.0000
X_1^2	1	1.0065	1.0065	10,065.27	0.0000
X_2	1	0.5320	0.5320	5319.940	0.0000
X_2^2	1	1.6335	1.6335	16,334.75	0.0000
X_3	1	0.6818	0.6818	6817.60	0.0000
X_3^2	1	2.3247	2.3247	23,247.26	0.0000
X_1X_2	1	0.1953	0.1953	1953.13	0.0000
X_1X_3	1	0.9730	0.9730	9730.13	0.0000
X_2X_3	1	0.1128	0.1128	1128.13	0.0000
Lack-of-fit	5	0.1704	0.0341	340.85	0.0000
Pure error	8	0.0008	0.0001	-	-
Total	22	12.2954	-	-	-

Table 7. ANOVA results for d_{001} of YB.

Term	DF	SS	MS	F	*p*-Value
X_1	1	5.2120	5.2120	46,907.69	0.0000
X_1^2	1	0.9322	0.9322	8339.84	0.0000
X_2	1	0.3594	0.3594	3234.52	0.0000
X_2^2	1	1.5384	1.5384	13,845.63	0.0000
X_3	1	0.9131	0.9131	8218.11	0.0000
X_3^2	1	2.2110	2.2110	19,899.30	0.0000
X_1X_2	1	0.0780	0.0780	702.11	0.0000
X_1X_3	1	0.6786	0.6786	6107.51	0.0000
X_2X_3	1	0.0406	0.0406	365.51	0.0000
Lack-of-fit	5	0.2139	0.0427	385.00	0.0000
Pure error	8	0.0009	0.0001	-	-
Total	22	12.1171	-	-	-

Tables 8 and 9 present the estimated effects and coefficients of the factors for d_{001} in WB and YB, respectively. As shown in the Pareto charts, temperature had the most significant impact on the degree of intercalation, followed by stirring speed and contact time.

Table 8. Effect estimates for d_{001} of WB.

Term	Effect	Coeff.	SE Coeff.	T	*p*-Value
Constant	3.78695	3.78695	0.00333	1136.83	0.0000
X_1	1.17696	0.58848	0.00271	217.47	0.0000
X_2	0.39474	0.19737	0.00271	72.938	0.0000
X_3	0.44686	0.22343	0.00271	82.569	0.0000
${X_1}^2$	−0.50337	−0.25169	0.00251	−100.33	0.0000
${X_2}^2$	−0.64126	−0.32063	0.00251	−127.81	0.0000
${X_3}^2$	−0.76500	−0.38250	0.00251	−152.47	0.0000
X_1X_2	0.31250	0.15625	0.00354	44.194	0.0000
X_1X_3	−0.69750	−0.34875	0.00354	−98.641	0.0000
X_2X_3	0.23750	0.11875	0.00354	33.588	0.0000
		R^2 = 98.61%	R^2(adj) = 97.64%		

Table 9. Effect estimates for d_{001} of YB.

Term	Effect	Coeff.	SE Coeff.	T	*p*-Value
Constant	3.82703	3.82703	0.00351	1089.91	0.0000
X_1	1.23554	0.61777	0.00285	216.82	0.0000
X_2	0.32444	0.16222	0.00285	56.873	0.0000
X_3	0.51715	0.25858	0.00285	90.654	0.0000
${X_1}^2$	−0.48443	−0.24222	0.00264	−91.596	0.0000
${X_2}^2$	−0.62232	−0.31116	0.00264	−117.667	0.0000
${X_3}^2$	−0.74606	−0.37303	0.00264	−141.065	0.0000
X_1X_2	0.19750	0.09875	0.00373	26.497	0.0000
X_1X_3	−0.58250	−0.29125	0.00373	−78.151	0.0000
X_2X_3	0.14250	0.07125	0.00373	19.118	0.0000
		R^2 = 98.23%	R^2(adj) = 97.00%		

The main effects of the linear terms for both clays displayed positive values, indicating that their presence in the process contributes to an increase in d_{001}. However, the quadratic terms showed negative values, suggesting that, despite being statistically significant, they help in a reduction in d_{001}. This implies that higher levels of these three factors lead to this reduction.

The interaction effects between temperature and stirring speed also showed negative values, indicating that, while both factors individually play a significant role in increasing d_{001}, their combination leads to a decrease.

3.6. Optimization of the Organo-Modification Conditions

Figures 6 and 7 show the response surfaces and contour plots depicting the dependency of temperature and agitation on d_{001} for the two clays, generated with Statsoft Statistica 8. The presence of curvatures indicates a significant and relevant interaction effect between temperature and agitation. This is consistent with the conclusions drawn from the evaluation of interaction effects using the Pareto charts (Figure 5), as well as from the ANOVA and estimated effects tables (Tables 6–9). As expected, Figure 7 confirms that d_{001} is influenced by both temperature and agitation speed, with the increase in d_{001} being notably more sensitive to temperature rise than to changes in agitation speed. At very high agitation speeds, d_{001} tends to decrease. These outcomes align with the data in Tables 8 and 9, which confirm that d_{001} is more responsive to changes in temperature. In both clays, temperature increases result in nearly a 1.2% rise in d_{001} compared to an approximately 0.5% increase in agitation speed. This fact is further supported by the higher temperature coefficient, which is twice as large as that of the stirring speed factor.

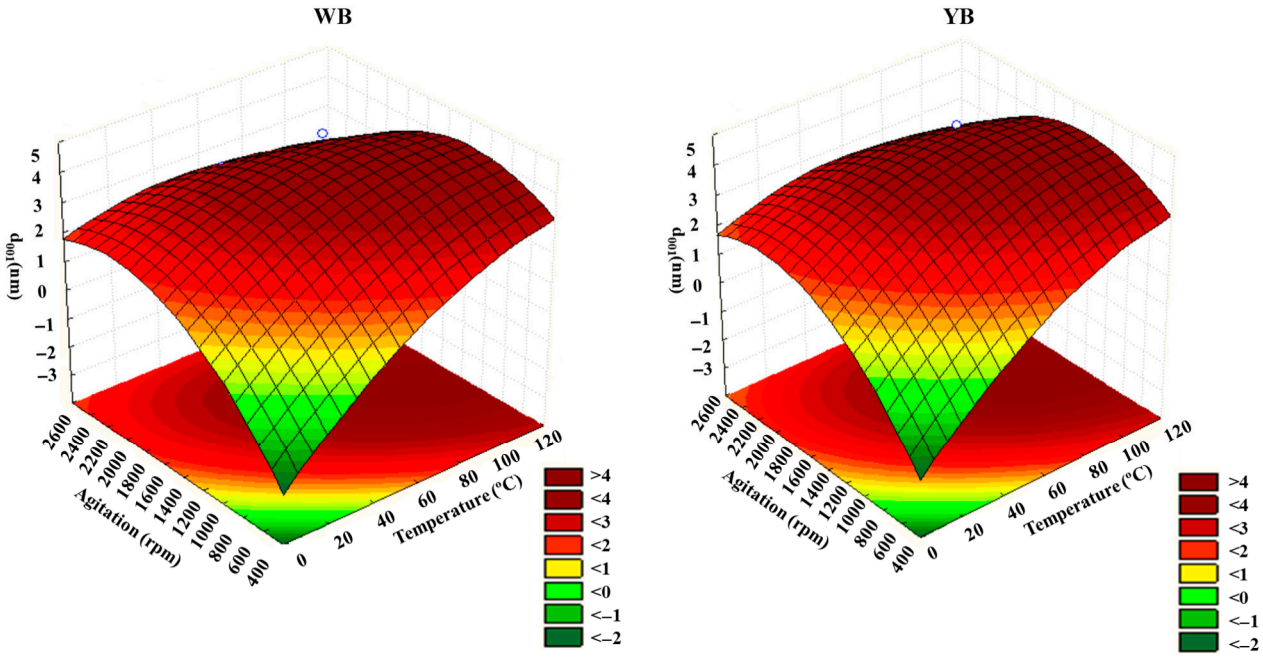

Figure 6. Response surface plots dependency of temperature and stirring speed on d_{001} for WB and YB (The white dots represent the levels of the factors used during the experiment, including the critical points).

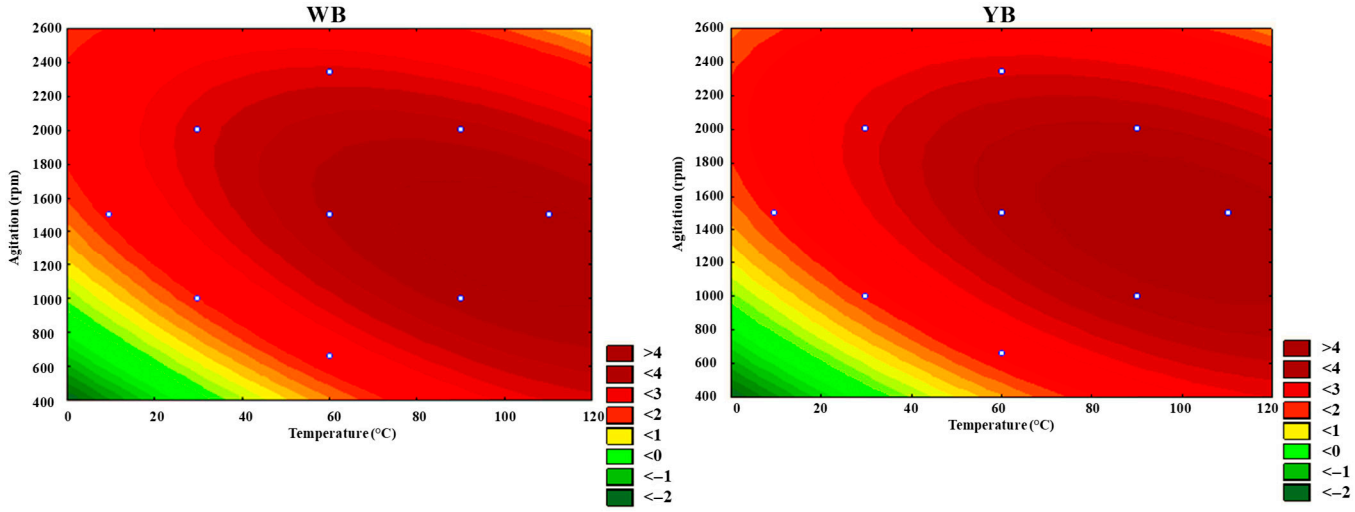

Figure 7. The contour plots show the relationship between temperature and stirring speed on d_{001} for WB and YB (The white dots represent the levels of the factors used during the experiment, including the critical points).

From Figure 7, it can be observed that optimal d_{001} values can be obtained in the range of temperature of 60 to 120 °C and stirring speeds between 1000 and 2000 rpm. Under these conditions, d_{001} reaches a maximum of around 4 nm.

The increased d_{001} with increasing temperatures can be attributed essentially to three factors: (a) Molecular mobility: Higher temperatures raise the kinetic energy of both the polyamide chains and the clay particles, likely increasing the mobility and reactivity of the amine groups, enabling them to penetrate the interlayer spaces of bentonite clay more easily; (b) Swelling thermodynamics: Bentonite clay, a layered material, experiences swelling when interacting with water or organic solvents [13,14,58]. High temperatures promote better swelling of the clay layers in the polymer solution, creating more space for polymer chains to intercalate; and (c) Reduced viscosity: Rising temperatures enhance the

solubility of the polymer solution in acetic acid by disrupting hydrogen bonds, which leads to a reduction in viscosity. The lower viscosity enhances the diffusion of polyamide chains, facilitating their movement into the interlayer spaces of the bentonite.

The increase in intercalation degree with higher stirring speeds is primarily due to the following factors: (a) Enhanced mass transfer: Faster stirring improves the interaction between polyamide chains in the solution and the clay surface by disrupting stagnant layers around the clay particles. The polymer chains penetrate more effectively into the clay's interlayer space, and (b) improved mixing and distribution: Agitation ensures the even distribution of polyamide chains throughout the mixture, preventing clay particle settling.

As previously mentioned, at very high stirring speeds, d_{001} tends to decrease. Figure 7 shows that above 2000 rpm, d_{001} decreases, indicating that the increase in d_{001} is affected at such high speeds. Although increasing stirring speed generally promotes intercalation, Figure 7 shows that at speeds above 2000 rpm, d_{001} begins to decrease. This suggests that excessively high shear forces generated at such speeds may disrupt the intercalated structure or cause mechanical degradation of the polymer chains, such as chain scission. A recent study by Morelly and co-workers [59], combining theoretical analysis and experimental results, demonstrated that increasing the shear rate during the mixing of polymers and particles leads to polymer chain scission, resulting in reduced molecular weight and viscosity.

Figures 8 and 9 illustrate the response surfaces and contour plots that demonstrate how the temperature and contact time of the two clays influence d_{001}. The curvature of the response surfaces and contour lines indicates a significant interaction effect between these two factors, as evidenced by the data presented in Tables 6–9. Optimal d_{001} values were obtained at a temperature range of 60 to 120 °C and a contact time between 30 and 90 min. Under these conditions, d_{001} also reaches a maximum of approximately 4 nm.

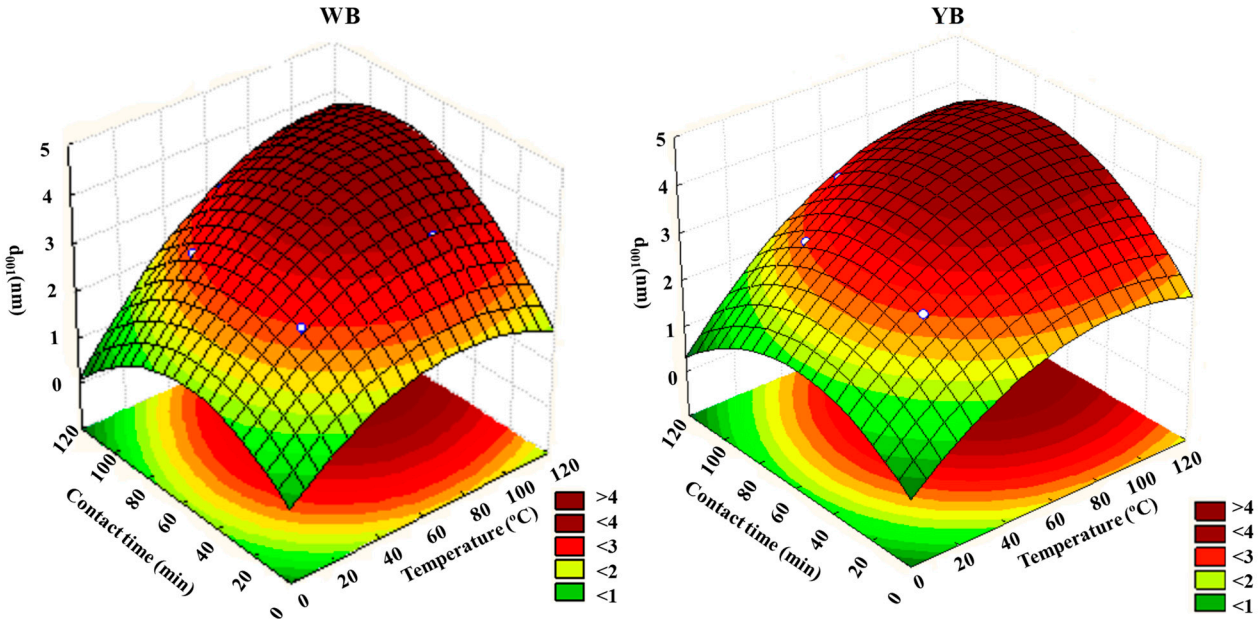

Figure 8. Response surface plots dependency of temperature and contact time on d_{001} for WB and YB (The white dots represent the levels of the factors used during the experiment, including the critical points).

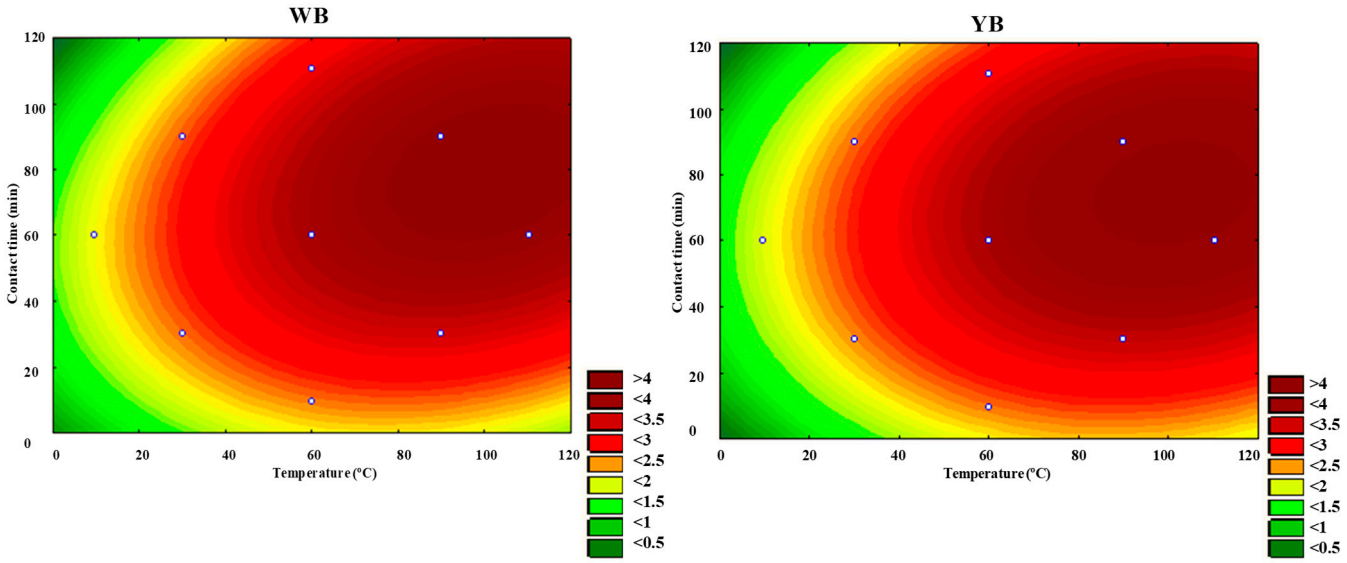

Figure 9. The contour plots show the relationship between temperature and contact time on d_{001} for WB and YB (The white dots represent the levels of the factors used during the experiment, including the critical points).

From Tables 8 and 9, it is clear that simultaneous heating and contact time confers a positive effect on d_{001}. However, the increase in d_{001} appears to be more sensitive to increasing temperature than contact time.

Contact time has a relatively minor impact on the organo-modification process compared to temperature and stirring speed. The time impact on the organo-modification process can be attributed to the saturation of intercalation and kinetic limitations, as explained in studies related to polymer crystallization and intercalation phenomena [60–62]. Temperature and agitation possess a stronger impact on the degree of intercalation. This suggests that under suitable temperature and agitation conditions, the system reaches equilibrium relatively quickly. At this point, the availability of polymer chains to access the interlayer spaces seems to become a limiting factor, rather than the duration of diffusion. Therefore, extending the contact time is unlikely to further influence the intercalation process once the chains have already entered the interlayer spaces.

The sensitivity of d_{001} to temperature increase may be linked to the low molecular mass of bio-based polyamides, influenced by its glass transition temperature (Tg). Below Tg, polymer chains are restricted in their movement, making the polymer rigid, while above Tg, the chains gain mobility, increasing flexibility [63,64]. This demonstrates that Tg is the boundary between low and high molecular mobility. Dimer fatty acid-based polyamides have a very low Tg, around 10 °C [41,42], which explains why any rise in temperature results in an increase in d_{001}. Additionally, the polymer being in solution may further enhance chain segment mobility. The presence of solvent molecules disrupts the polymer chains' intermolecular interactions, reducing the energy barrier for segmental motion, hence, enhanced mobility of polymer chains, enabling them to move more freely at lower temperatures compared to the pure polymer. The solvent acts as a plasticizer by inserting itself between the polymer chains, effectively lowering the Tg by reducing the rigidity of the polymer structure [65–67].

Figures 10 and 11 illustrate the response surfaces and contour plots that demonstrate how contact time and agitation of the two clays influence d_{001}. The curvature of the response surfaces and contour lines indicate a significant interaction effect between these two factors, as evidenced by the data presented in Tables 6–9.

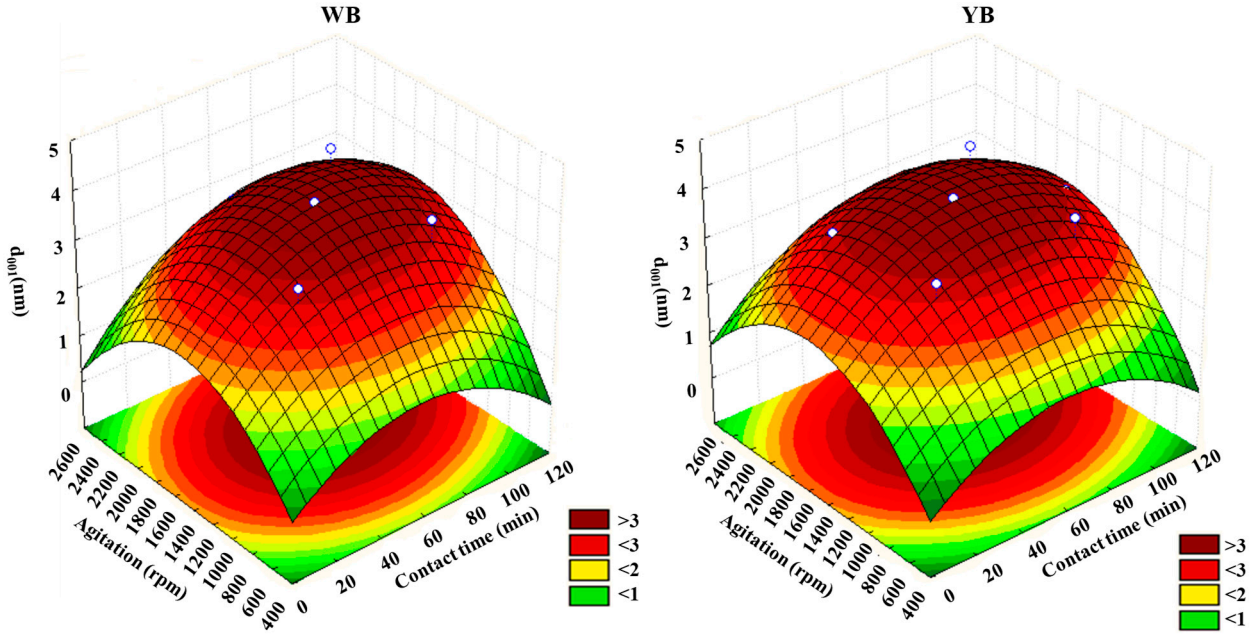

Figure 10. Response surface plots dependency of agitation and contact time on d_{001} for WB and YB (The white dots represent the levels of the factors used during the experiment, including the critical points).

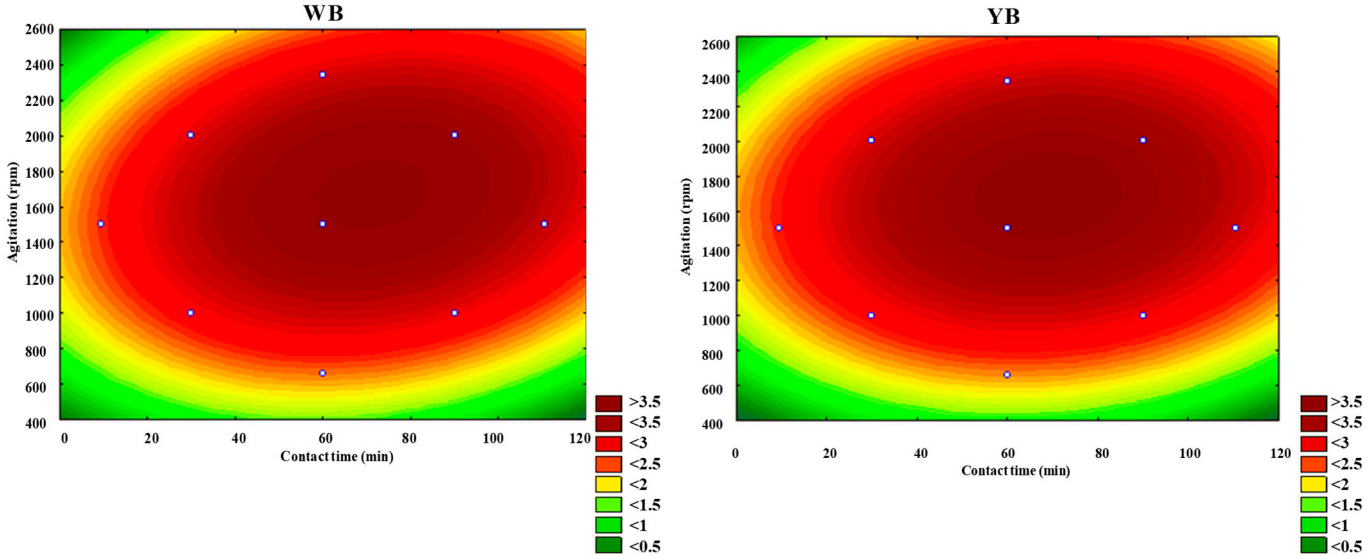

Figure 11. The contour plots show the relationship between agitation and contact time on d_{001} for WB and YB (The white dots represent the levels of the factors used during the experiment, including the critical points).

Although the combination of agitation and contact time contributes to an increase in d_{001}, the effect is relatively modest compared to other factor combinations, such as temperature with agitation speed or temperature with contact time. This is consistent with the results in Tables 8 and 9, which demonstrate that, in absolute terms, the combination of agitation speed and contact time has a smaller impact on the increase in d_{001}. Optimal d_{001} values can be achieved with stirring speeds between 1200 and 2000 rpm and contact times ranging from 50 to 90 min.

Table 10 presents the stationary points for the maximum values of d_{001} for both WB and YB clays. On average, the maximum d_{001} is achieved at approximately 105 °C, with a contact time of 75 min and a stirring speed of 1400 rpm. These values are within the range of the independent variables under investigation. Under these conditions, d_{001} for both

clays reaches a maximum of about 4 nm. However, the analysis of the response surface and contour plots suggests that this maximum can also be attained at 90 °C, with a stirring speed of 1500 rpm and a contact time of 60 min.

Table 10. Stationary points for the maximum values of d_{001} for both WB and YB clays.

Factor	Minimum d_{001}	Critical Values	Maximum d_{001}
Z_1 (WB)	9.5462	108.040	110.454
Z_2 (WB)	9.5462	79.054	110.454
Z_3 (WB)	659.1036	1330.315	2340.896
Z_1 (YB)	9.5462	104.547	110.454
Z_2 (YB)	9.5462	74.244	110.454
Z_3 (YB)	659.1036	1406.124	2340.896

Based on the analysis shown in Tables 8 and 9, it is evident that temperature, stirring speed, and contact time impact the degree of polymer chain intercalation into clay galleries. XRD analysis demonstrated that the d_{001} spacing increased from 1.73 nm to 3.79 nm for WB and from 1.77 nm to 3.83 nm for YB, as the organo-modification temperature, contact time, and stirring speed were adjusted from 30 to 90 °C, 30 to 90 min, and 1000 to 2000 rpm, respectively. Similar *d*-spacings were reported for Boane's white organo-bentonites [32]. These were organo-bentonite samples containing quaternary ammonium surfactants that were purified and modified with soda ash. The *d*-spacings of 1.73 and 1.77 nm to approximately 4 nm observed in the two clays indicate the presence of lateral bilayer, pseudotrimolecular layer, and paraffin-type bilayer structures [18,32,53].

Plots of the standardized residuals with normal probability are commonly used to evaluate how well the fitted model represents the real system. Figure 12 displays the graphs for d_{001}, where most of the data points align with the straight line or predicted data, suggesting that the errors are attributed to a normal distribution for many responses.

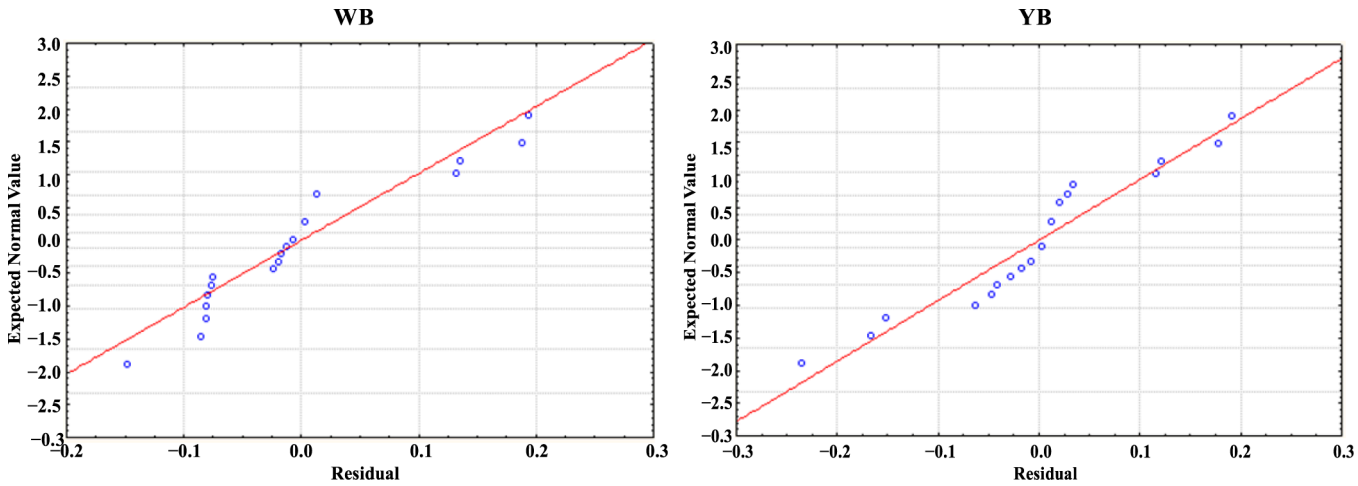

Figure 12. Normal probability plots of d_{001} for both WB and YB.

3.7. Statistical Design Model

Statistical experimental design was utilized to build a second-order regression model, as outlined in Equation (1). The model was constructed based on the coded variables derived from the coefficients and effect estimates for d_{001}, shown in Tables 8 and 9. Using the coefficients from column 3 of these tables, Equations (8) and (9) were developed to serve as a representation of the statistical design model for d_{001} of the variables (X_i). All terms, including linear, quadratic, and interaction effects for the two clays, were significant

at the 95% confidence level and were therefore incorporated into the respective models, as illustrated below.

$$d_{001}(WB) = 3.787 + 0.588X_1 + 0.197X_2 + 0.223X_3 - 0.252{X_1}^2 - 0.321{X_2}^2 - 0.383{X_3}^2 + 0.156X_1X_2 - 0.349X_1X_3 + 0.119X_2X_3 \quad (8)$$

and

$$d_{001}(YB) = 3.827 + 0.618X_1 + 0.162X_2 + 0.259X_3 - 0.242{X_1}^2 - 0.311{X_2}^2 - 0.373{X_3}^2 + 0.099X_1X_2 - 0.291X_1X_3 + 0.071X_2X_3 \quad (9)$$

Figure 13 compares the experimental and predicted d_{001} values based on statistical design models (Equations (8) and (9)), with R^2 values of 0.9861 for WB and 0.9823 for YB, indicating satisfactory predictive accuracy for d_{001}.

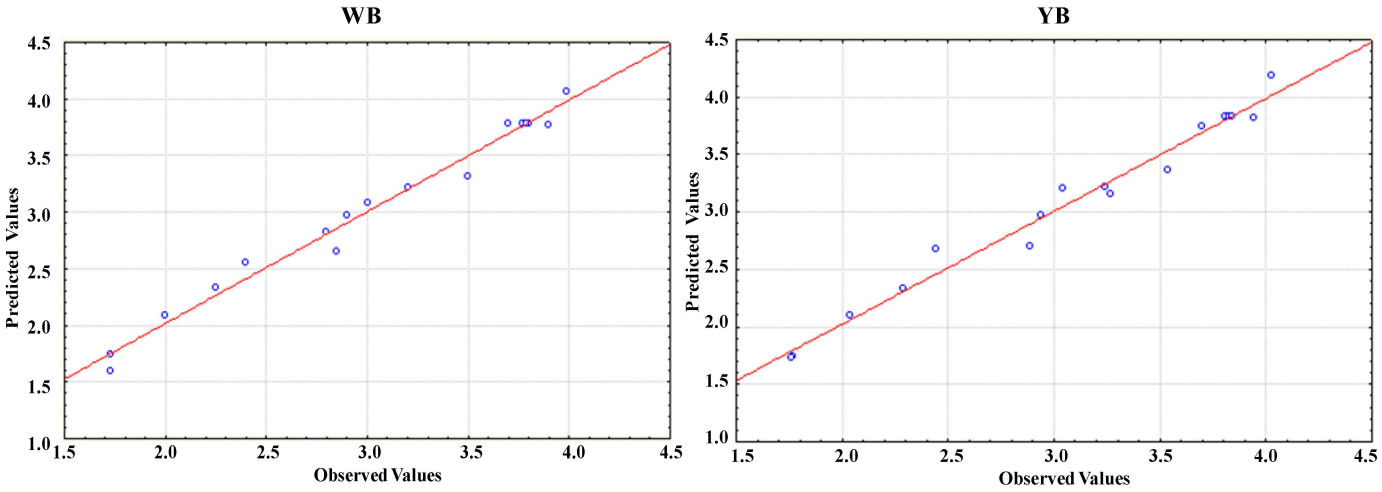

Figure 13. Predicted values versus experimental values plots of d_{001} for both WB and YB.

4. Conclusions

This study explored the preparation of bentonite bio-organoclays using protonated dimer acid-based polyamine chains, synthesized from two Mozambican montmorillonite clays via a solution casting technique. XRD analysis confirmed the successful intercalation of polyamide chains within the clay interlayer spaces, indicated by an increase in d_{001} values. In the initial stage of the experiment, varying polymer concentrations at a constant temperature (30 °C), contact time (30 min), and stirring speed (1000 rpm) resulted in limited intercalation, with d_{001} values reaching only 1.7 nm, compared to initial values of approximately 1.5 nm for both clays. This indicated that polymer concentration did not strongly influence the process. The limited intercalation could be attributed to the formation of agglomerates of the clays observed by SEM. However, in the second stage, where temperature (30–90 °C), contact time (30–90 min), and stirring speed (1000–2000 rpm) were varied while maintaining constant polymer concentration, significant increases in d_{001} were observed, achieving values around 4 nm. Statistical Design Modeling and Response Surface Methodology revealed that all factors and their effects of interactions significantly influenced d_{001} in a 95% degree of confidence, with temperature and stirring speed having a greater impact than contact time. The optimal activation conditions for maximum d_{001} (4 nm) were determined to be at 90 °C, a stirring speed of 1500 rpm, and a contact time of 60 min.

Additionally, the predictive statistical model exhibited a strong linear relationship with R^2 of 0.9861 for WB and 0.9823 for YB, demonstrating high predictive accuracy for d_{001}. Finally, the combination of bentonite with polyamide was regarded as highly significant, as it facilitated the development of bentonite-based bio-organoclays that minimize or eliminate harmful effects on humans, animals, and the environment. Furthermore, the statistical design model

employed in this study proved effective for predicting the optimal processing and preparation conditions required to obtain bio-organoclays with the desired material properties—an important consideration for scaling up these materials for practical applications.

Author Contributions: Conceptualization, A.D.M.; Data curation, A.D.M. and A.B.M.; Formal analysis, A.D.M., R.K.T., A.B.M. and S.M.T.; Funding acquisition, A.D.M. and S.M.T.; Investigation, A.D.M., D.N.M., T.M.M., A.B.M. and S.M.T.; Methodology, A.D.M., D.N.M. and T.M.M.; Project administration, A.D.M. and S.M.T.; Software, A.D.M.; Validation, A.D.M., D.N.M., T.M.M., R.K.T., A.B.M. and S.M.T.; Visualization, R.K.T. and A.B.M.; Writing—original draft, A.D.M., A.B.M. and R.K.T.; Writing—review and editing, A.D.M., D.N.M., T.M.M., R.K.T., A.B.M. and S.M.T. All authors have read and agreed to the published version of the manuscript.

Funding: This research was funded by the World Bank Group, through the Eastern and Southern Africa Higher Education Centres of Excellence Project Initiative (ACE II), and the National Research Foundation (NRF) of South Africa, grant number TTK18024324064.

Data Availability Statement: The original contributions presented in this study are included in the article. Further inquiries can be directed to the corresponding author.

Conflicts of Interest: The authors declare no conflicts of interest.

References

1. Murray, H.H. Traditional and new applications for kaolin, smectite, and palygorskite: A general overview. *Appl. Clay Sci.* **2000**, *17*, 207–221. [CrossRef]
2. Allo, W.A.; Murray, H.H. Mineralogy, chemistry and potential applications of a white bentonite in San Juan province, Argentina. *Appl. Clay Sci.* **2004**, *25*, 237–243. [CrossRef]
3. Murray, H.H. Bentonite applications. *Dev. Clay Sci.* **2006**, *2*, 111–130.
4. Murray, H.H. Industrial clays case study. *Min. Miner. Sustain. Dev.* **2002**, *64*, 1–9.
5. De Azeredo, H.M.C. Nanocomposites for food packaging applications. *Food Res. Int.* **2009**, *42*, 1240–1253. [CrossRef]
6. Ayari, F.; Srasra, E.; Trabelsi-Ayadi, M. Characterization of bentonitic clays and their use as adsorbent. *Desalination* **2005**, *185*, 391–397. [CrossRef]
7. Bahranowski, K.; Klimek, A.; Gaweł, A.; Serwicka, E.M. Rehydration Driven Na-Activation of Bentonite—Evolution of the Clay Structure and Composition. *Materials* **2021**, *14*, 7622. [CrossRef] [PubMed]
8. Christidis, G.E. The concept of layer charge of smectites and its implications for important smectite-water properties. In *Layered Mineral Structures and Their Application in Advanced Technologies*; European Mineralogical Union: Paris, France, 2011.
9. Del Hoyo, C. Layered double hydroxides and human health: An overview. *Appl. Clay Sci.* **2007**, *36*, 103–121. [CrossRef]
10. Bergaya, F.; Lagaly, G. Surface modification of clay minerals. *Appl. Clay Sci.* **2001**, *19*, 1–3. [CrossRef]
11. Magzoub, M.I.; Hussein, I.A.; Nasser, M.S.; Mahmoud, M.; Sultan, A.S.; Benamor, A. An investigation of the swelling kinetics of bentonite systems using particle size analysis. *J. Dispers. Sci. Technol.* **2019**, *41*, 817–827. [CrossRef]
12. Mapossa, A.B.; da Silva Júnior, A.H.; de Oliveira, C.R.S.; Mhike, W. Thermal, Morphological and Mechanical Properties of Multifunctional Composites Based on Biodegradable Polymers/Bentonite Clay: A Review. *Polymers* **2023**, *15*, 3443. [CrossRef]
13. Alther, G. Some practical observations on the use of bentonite. *Environ. Eng. Geosci.* **2004**, *10*, 347–359. [CrossRef]
14. Inglethorpe, S.D.J.; Morgan, D.J.; Highley, D.E.; Bloodworth, A.J. *Industrial Minerals laboratory manual: Bentonite*; British Geological Survey Technical Report WG/93/20; British Geological Survey: Nottingham, UK, 1993.
15. Favre, H.; Lagaly, G. Organo-bentonites with quaternary alkylammonium ions. *Clay Miner.* **1991**, *26*, 19–32. [CrossRef]
16. Barrer, R.M.; Macleod, D.M. Intercalation and sorption by montmorillonite. *Trans. Faraday Soc.* **1954**, *50*, 980–989. [CrossRef]
17. Barrer, R.M.; Macleod, D.M. Activation of montmorillonite by ion exchange and sorption complexes of tetra-alkyl ammonium montmorillonites. *Trans. Faraday Soc.* **1955**, *51*, 1290–1300. [CrossRef]
18. Lazorenko, G.; Kasprzhitskii, A.; Yavna, V. Comparative study of the hydrophobicity of organo-montmorillonite modified with cationic, amphoteric and nonionic surfactants. *Minerals.* **2020**, *10*, 732. [CrossRef]
19. Sompech, S.; Nuntiya, A.; Aukkaravittayapun, S.; Pumchusak, J. Interlayer expansion of organoclay by cationic surfactant. *Chiang Mai Univ. J. Nat. Sci. Spec. Issue Nanotechnol.* **2008**, *7*, 89–93.
20. Fink, J. *Water-Based Chemicals and Technology for Drilling, Completion, and Workover Fluids*; Gulf Professional Publishing: Oxford, UK, 2015.
21. Sarkar, B.; Rusmin, R.; Ugochukwu, U.C.; Mukhopadhyay, R.; Manjaiah, K.M. Modified clay minerals for environmental applications. In *Modified Clay and Zeolite Nanocomposite Materials*; Elsevier: Amsterdam, The Netherlands, 2019; pp. 113–127.

22. Leyva-Ramos, R.; Jacobo-Azuara, A.; Martínez-Costa, J.I. Organoclays. Fundamentals and Applications for Removing Toxic Pollutants from Water Solution. In *Porous Materials*; Springer: Cham, Switzerland, 2021; pp. 341–363.
23. Lagaly, G. Clay-organic interactions. *Philos. Trans. A Math. Phys. Eng. Sci.* **1984**, *311*, 315–332.
24. Lagaly, G. Interaction of alkylamines with different types of layered compounds. *Solid State Ion.* **1986**, *22*, 43–51. [CrossRef]
25. Mortland, M.M.; Shaobai, S.; Boyd, S.A. Clay-organic complexes as adsorbents for phenol and chlorophenols. *Clay Miner.* **1986**, *34*, 581–585. [CrossRef]
26. Smith, J.A.; Jaffe, P.R.; Chiou, C.T. Effect of ten quaternary ammonium cations on tetrachloromethane sorption to clay from water. *J. Environ. Sci. Technol.* **1990**, *24*, 1167–1172. [CrossRef]
27. Alther, L.; Stege, G. *Hautkontakte: Roman*; Ullstein: Berlin, Germany, 1992.
28. Boyd, S.A.; Guangyao, S.; Teppen, B.J.; Johnson, C.T. Mechanisms for the adsorption of substituted nitrobenzenes by smectite clays. *J. Environ. Sci. Technol.* **2001**, *35*, 4227–4234. [CrossRef]
29. Alther, G. Using organoclays to enhance carbon filtration. *J. Waste Manag.* **2002**, *22*, 507–513. [CrossRef] [PubMed]
30. Lee, S.Y.; Kim, S.J. Expansion characteristics of organoclay as a precursor to nanocomposites. *Colloids Surf. A Physicochem. Eng. Asp.* **2002**, *211*, 19–26. [CrossRef]
31. Sanchez-Martin, M.J.; Rodriguez-Cruz, M.S.; Andrades, M.S.; Sanchez-Camazano, M. Efficiency of different clay minerals modified with a cationic surfactant in the adsorption of pesticides: Influence of clay type and pesticide hydrophobicity. *Appl. Clay Sci.* **2006**, *31*, 216–228. [CrossRef]
32. De Paiva, L.B.; Morales, A.R.; Díaz, F.R.V. Organoclays: Properties, preparation and applications. *Appl. Clay Sci.* **2008**, *42*, 8–24. [CrossRef]
33. He, H.; Ma, Y.; Zhu, J.; Yuan, P.; Qing, Y. Organoclays prepared from montmorillonites with different cation exchange capacity and surfactant configuration. *Appl. Clay Sci.* **2010**, *48*, 67–72. [CrossRef]
34. Massinga, P.H., Jr.; Focke, W.W.; De Vaal, P.L.; Atanasova, M. Alkyl ammonium intercalation of Mozambican bentonite. *Appl. Clay Sci.* **2010**, *49*, 142–148. [CrossRef]
35. Negin, C.; Ali, S.; Xie, Q. Most common surfactants employed in chemical enhanced oil recovery. *Petroleum* **2017**, *3*, 197–211. [CrossRef]
36. Guégan, R.; Veron, E.; Le Forestier, L.; Ogawa, M.; Cadars, S. Structure and Dynamics of Nonionic Surfactant Aggregates in Layered Materials. *Langmuir* **2017**, *33*, 9759–9771. [CrossRef]
37. Guégan, R. Organoclay applications and limits in the environment. *Comptes Rendus Chim.* **2019**, *22*, 132–141. [CrossRef]
38. Macheca, A.D.; Uwiragiye, B. Application of Nanotechnology in Oil and Gas Industry: Synthesis and Characterization of Organo-modified Bentonite from Boane Deposit and its Application in Produced Water Treatment. *Chem. Eng. Trans.* **2020**, *81*, 1081–1086.
39. Murtaza, M.; Kamal, M.S.; Hussain, S.M.S.; Mahmoud, M.; Syed, N.A. Quaternary ammonium gemini surfactants having different spacer length as clay swelling inhibitors: Mechanism and performance evaluation. *J. Mol. Liq.* **2020**, *308*, 113054. [CrossRef]
40. Ray, S.S. *Environmentally Friendly Polymer Nanocomposites: Types, Processing and Properties*; Elsevier: Amsterdam, The Netherlands, 2013; pp. 3–24.
41. Macheca, A.; Gnanasekaran, D.; Focke, W.W. Surfactant-free dimer fatty acid polyamide/montmorillonite bio-nanocomposites. *Colloid Polym. Sci.* **2014**, *292*, 669–676. [CrossRef]
42. Macheca, A.D.; Focke, W.W.; Muiambo, H.F.; Kaci, M. Stiffening mechanisms in vermiculite–amorphous polyamide bio-nanocomposites. *Eur. Polym. J.* **2016**, *74*, 51–63. [CrossRef]
43. Macheca, A.D.; Focke, W.W.; Kaci, M.; Panampilly, B.; Androsch, R. Flame retarding polyamide 11 with exfoliated vermiculite nanoflakes. *Polym. Eng. Sci.* **2018**, *58*, 1746–1755. [CrossRef]
44. Macheca, A.D.; Mapossa, A.B.; Cumbane, A.J.; Sulemane, A.E.; Tichapondwa, S.M. Development and Characterization of Na_2CO_3-Activated Mozambican Bentonite: Prediction of Optimal Activation Conditions Using Statistical Design Modeling. *Minerals* **2022**, *12*, 1116. [CrossRef]
45. Brunauer, S.; Emmett, P.H.; Teller, E. Adsorption of gases in multimolecular layers. *J. Am. Chem. Soc.* **1938**, *60*, 309–319. [CrossRef]
46. Montgomery, D.C. *Montgomery Design and Analysis of Experiments*, 8th ed.; John Wiley & Sons, Inc.: Sedona, AZ, USA, 2013; pp. 65–553.
47. Nemukula, A.; Mutanda, T.; Wilhelmi, B.S.; Whiteley, C.G. Response surface methodology: Synthesis of short chain fructooligosaccharides with a fructosyltransferase from Aspergillus aculeatus. *Bioresour. Technol.* **2009**, *100*, 2040–2045. [CrossRef]
48. Lee, K.E.; Morad, N.; Teng, T.T.; Poh, B.T. Evaluation of factors and kinetics study of polyacrylamide redox polymerization using statistical design modeling. *J. Polym. Eng.* **2012**, *32*, 215–224. [CrossRef]
49. Grim, R.E.; Guven, N. *Bentonites: Geology, Mineralogy, Properties and Uses*; Elsevier: Amsterdam, The Netherlands, 2011.
50. Dos Muchangos, A.C.D. Mineralogy and Geochemistry of Bauxite and Bentonite Deposits from Mozambique. Doctoral Thesis, Utrecht University, Utrecht, The Netherlands, 2000.
51. Cílek, V. *Industrial minerals of Mozambique*, 1st ed.; Czech Geological Office: Prague, Czech Republic, 1989; pp. 143–149.

52. Holmboe, M.; Wold, S.; Jonsso, M. Porosity investigation of compacted bentonite using XRD profile modeling. *J. Contam. Hydrol.* **2012**, *128*, 19–32. [CrossRef] [PubMed]
53. Breakwell, I.K.; Homer, J.; Lawrence, M.A.; Mcwhinnie, W.R. Studies of organophilic clays: The distribution of quaternary ammonium compounds on clay surfaces and the role of impurities. *Polyhedron* **1995**, *14*, 2511–2518. [CrossRef]
54. Lehto, T.; Gonçalves, R. *Mineral Resources Potential in Mozambique*; Special Paper; Geological Survey of Finland: Espoo, Finland, 2008; Volume 48, pp. 307–321.
55. Mackenzie, R.C. *Differential Thermal Analysis Academic I, II*; Academic Press: New York, NY, USA, 1970.
56. Xie, W.; Gao, Z.; Pan, W.P.; Hunter, D.; Singh, A.; Vaia, R. Thermal degradation chemistry of alkyl quaternary ammonium montmorillonite. *Chem. Mater.* **2001**, *13*, 2979–2990. [CrossRef]
57. Praus, P.; Turicová, M.; Študentová, S.; Ritz, M. Study of cetyltrimethylammonium and cetylpyridinium adsorption on montmorillonite. *J. Colloid Interface Sci.* **2006**, *304*, 29–36. [CrossRef]
58. Foster, M.D. The relation between composition and swelling in clays. *Clays Clay Miner.* **1954**, *3*, 205–220. [CrossRef]
59. Morelly, S.L.; Saraka, R.M.; Alvarez, N.J.; Tang, M. Impact of Mixing Shear on Polymer Binder Molecular Weight and Battery Electrode Reproducibility. *Batteries* **2024**, *10*, 46. [CrossRef]
60. Laipan, M.; Xiang, L.; Yu, J.; Martin, B.R.; Zhu, R.; Zhu, J.; He, H.; Clearfield, A.; Sun, L. Layered intercalation compounds: Mechanisms, new methodologies, and advanced applications. *Prog. Mater. Sci.* **2020**, *109*, 100631. [CrossRef]
61. Vedantam, S.; Ranade, V.V. Crystallization: Key thermodynamic, kinetic and hydrodynamic aspects. *Sadhana* **2013**, *38*, 1287–1337. [CrossRef]
62. Zlatkevich, L.; Zlatkevich, L. Molecular Mobility and Transitions in Polymers. In *Radiothermoluminescence and Transitions in Polymers*; Springer: New York, NY, USA, 1987; pp. 55–80.
63. What Is Glass Transition Temperature (Tg). Available online: https://adhetron.com/what-is-glass-transition-temperature-tg/ (accessed on 5 October 2024).
64. Understanding the Glass Transition Temperature of Polymers. Available online: https://polymer-search.com/understanding-the-glass-transition-temperature-of-polymers/ (accessed on 5 October 2024).
65. Polymer Chemistry: Factors Influencing Tg. Available online: https://eng.libretexts.org/Bookshelves/Materials_Science/Supplemental_Modules_(Materials_Science)/Polymer_Chemistry/Polymer_Chemistry:_Transitions/Polymer_Chemistry:_Factors_Influencing_Tg (accessed on 5 October 2024).
66. Sienkiewicz, A.; Krasucka, P.; Charmas, B.; Stefaniak, W.; Goworek, J. Swelling effects in cross-linked polymers by thermogravimetry. *J. Therm. Anal. Calorim.* **2017**, *130*, 85–93. [CrossRef]
67. Ligia, G.; Deodato, R. Polymer Solution Behavior: Polymer in Pure Solvent and in Mixed Solvent. In *Physicochemical Behavior and Supramolecular Organization of Polymers*; Springer: Dordrecht, The Netherlands, 2009; pp. 1–42.